Barrierless Isomerization Dynamics in Viscous Liquids: Decoupling of the Reaction Rate from the Slow Frictional Forces

R. Aldrin Denny

Solid State and Structural Chemistry Unit, Indian Institute of Science, Bangalore 560 012, India

Biman Bagchi*

Solid State and Structural Chemistry Unit, Indian Institute of Science, Bangalore 560 012, India, and Department of Chemistry, University of Wisconsin, Madison, Wisconsin 53706

Received: August 11, 1999

Many important chemical and biological reactions do not face a sizable activation barrier in their motion along the reaction coordinate. As a result, these reactions often have time constants in the range of a few hundred femtoseconds (fs) only. The existing theories, on the other hand, assume only the viscous, zero frequency frictional response of the solvent, which is clearly inadequate to describe solvent viscosity effects on such ultrafast reactions. In this article, we present a theory of barrierless chemical reactions that includes the bimodal frictional response of the solvent. The generalized theory is based on a non-Markovian Smoluchowski equation, with a time (t) dependent diffusion coefficient ($D(t)$) to describe the reactive motion along the reaction surface; the reaction itself is described by a coordinate-dependent sink term. This description is reliable for a harmonic reaction potential energy surface. The time-dependent diffusion coefficient can be obtained from the time-dependent friction by using the known procedure. The calculated rates show that the barrierless reaction rate becomes completely decoupled from slow solvent frictional forces when the rate of the reaction is large. This is particularly true for slow viscous liquids where the fast response of the liquid is vastly separated in a time scale from the slow response. For ultrafast reactions, this theory naturally leads to a fractional viscosity (η) dependence of the rate ($k \sim \eta^{-\alpha}$), with the value of the exponent α being close to zero at large solvent viscosities. The theory predicts excitation wavelength and temperature dependence in agreement with experiments. The results of the theory have been used to analyze and understand the experimental results of isomerization in rhodopsin, isorhodopsin, crystal violet, and several other cases.

I. Introduction

Many important chemical and biological reactions in solution occur without the intervention of any potential barrier to the reactive motion.[1,2] The dynamics of such barrierless reactions naturally differ considerably from those chemical reactions where the reactant has to climb a high activation barrier (E_{act}) to reach the product. The effects of solvent frictional forces on activated chemical reactions in solution have been studied theoretically by Kramers,[3] Grote−Hynes,[4] and Pollak.[5] Barrierless chemical reactions (with $E_{act} \leq 1$ kcal/mol) have drawn much less theoretical attention. Many activationless processes are found in the photoassisted isomerization. The most important example is certainly the transducting process *vision*, which involves a cis- to trans-transformation of the retinal chromophore.[6,7] Isomerizations of stilbene and diphenylbutadiene in alcohol solvents and of triphenylmethane dyes (crystal violet and ethyl violet) in lower alcohols are all known to follow barrierless reaction pathways.[8] Barrierless reactions are generally characterized by high reaction rates, exhibit a temperature dependence distinctly different from that of high barrier reactions, and are often strongly coupled to solvent viscosity. Actually, viscosity dependence has been often used to characterize the reaction mechanism of these reactions. Another important feature is that these reactions may depend on the initial conditions; thus, not only the wavelength of the excitation light but also the frequency of both the excited- and ground-state potential surfaces may play an important role in controlling the relaxation dynamics.

Recent advances in ultrafast laser spectroscopy have allowed the study of reactions hitherto impossible and have shown that the rates of isomerization reactions are often much larger than what was thought previously. For example, Peteanu and coworkers[9] have employed a 35 fs pump pulse and studied the rhodopsin isomerization using 10 fs probe pulses and showed the reaction dynamics (delay time $\approx$ 200 fs) is much faster than the previous reported value of 30 ps.[10] The femtosecond time-resolved spectroscopic study of Maruyama et al.[11] has also shown that the excited-state relaxation of crystal violet is complete within 500 fs and reported an anomalous viscosity dependence. A similar enhanced rate due to the higher resolution of recent femtosecond investigations has been noted in the isomerization of *cis*-stilbene by Sension et al.[12] and in tetraphenylethylene by Lenderink et al.[13]

A typical reaction potential energy surface for a barrierless reaction is depicted in Figure 1. The reaction is excited from the ground state to a position denoted by χ_0 on the excited-state surface. The subsequent relaxation brings the reactant down toward the potential energy minimum where the efficient sink χ_s is also located. This initial relaxation is resisted by solvent friction for those cases where relaxation involves large amplitude

* Corresponding author. Also at the Jawaharlal Nehru Centre for Advanced Scientific Research, Jakkur, Bangalore 560 012, India. Permanent address at the Indian Institute of Science.

10.1021/jp9928309 CCC: $18.00
Published on Web 10/26/1999

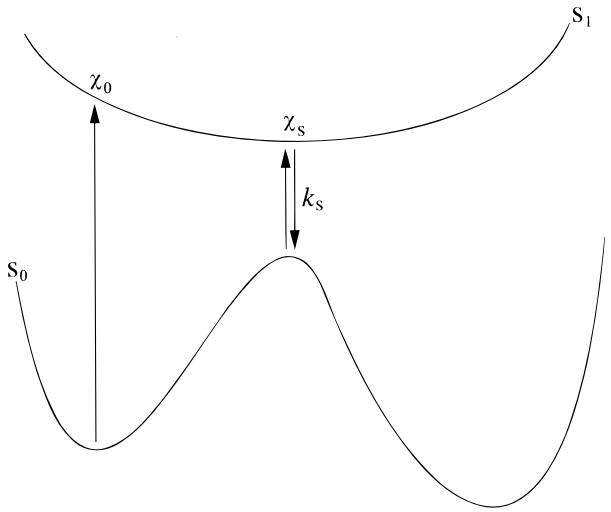

Figure 1. Schematic illustration of the physical processes involved in the study of barrierless isomerization reaction. The initial state (S_0) is the ground state of the isomerizing molecule. An instantaneous laser pulse transfers the population distribution to the excited state (S_1). The χ_0 in the S_1 surface indicates the excitation position. As the time increases, the population at χ_0 diffuses along the S_1 surface to reach the minimum, χ_s. The decay in the excited-state population from $S_1 \rightarrow S_0$ occurs at the sink which is present at the minimum of the S_1 surface. The dynamics of $S_1 \rightarrow S_0$ transition is controlled by the rate constant k_s.

motion, as is believed to be the case in cis−trans isomerization or in TPM dyes.

Several theories have been proposed to understand these astronishingly fast reactions.[8,14] A detailed theory of barrierless reaction was proposed by Bagchi et al.[15] In this model, sink is assumed to be coordinate-dependent for radiationless processes and a one-dimensional model for reactive motion on the excited state is introduced. The reactive motion along the S_1 surface is modeled by the damped motion of a Brownian particle on a harmonic surface. The motion along the potential surface is governed by the potential and the viscous drag of the solvent. This model suggests the rate of the barrierless reaction is a strong function of the viscosity of the medium.

A limitation of the Bagchi−Fleming−Oxtoby theory[15] (and of all other existing descriptions of barrierless isomerization reactions as well) is the use of an overdamped Markovian description of the dynamics. Thus, the response of the liquid to the motion of the reactant was assumed to be purely viscous. In the case of high barrier reactions, it is known that the viscous approximation of the friction leads to a completely wrong viscosity dependence.[4,16] A similar situation can arise in the case of those barrierless reactions that are very fast (with time constants in the subpicosecond range) and that may thus probe only the short time response of the solvent. This calls for a generalization of the existing theories of barrierless reactions in solution to include the bimodal response of the solvent.

In this article, we present such a generalized model for barrierless reactions by including the viscoelastic response of the medium. This requires a non-Markovian description of friction for the reactive motion. This is achieved by using the generalized Smoluchowski equation with a time-dependent diffusion coefficient, $D(t)$.[17] Such a description is valid for a harmonic reaction surface. Recent studies have shown that the time-dependent diffusion coefficient can have a value at short times which is quite different from that at the long times. In particular, the short time value of $D(t)$ is determined by the short time or the high-frequency frictional response of the solvent, which is again determined by the static correlations and hence by the local structure surrounding the reactant. This is to be contrasted with the long time diffusion which is often determined by the dynamical correlations. The friction at the long time is proportional to the slow, zero-frequency viscous response which might have no influence on ultrafast chemical reactions. The generalized Smoluchowski equation with a position-dependent reaction sink term has been solved by using Green's function technique.[18−21] The short and long time responses of the medium are introduced in the time-dependent friction expression, which is similar to the friction obtained by the mode-coupling theory calculation.[22] The main point here is that while the short time friction may make a much smaller contribution to the total zero-frequency friction than the slowly relaxing component, it might be the former that is really coupled to the ultrafast reaction.

We must mention here that a Smoluchowski equation description with time-dependent diffusion has been used earlier to treat dynamic solvent effects on electron-transfer reactions by Hynes,[23] by Gayathri and Bagchi,[21] and more recently by Bicout and Szabo.[24] Such a description, however, has not been used to treat viscosity dependence of barrierless reactions. Such a need of course arises mainly for ultrafast reactions.

The time profile of the survival probability calculated from this non-Markovian analysis shows a faster decay in the population distribution than what was observed in the Markovian theory. For the pinhole sink, the time dependence of survival probability is highly nonexponential and the decay is found to be complete even before a steady-state distribution is reached. Even for sinks with a finite decay rate, the decay is significantly nonexponential. One, of course, recovers an exponential decay in the long time when the decay rate from the sink is small, and this rate agrees with the one given by the Bagchi−Fleming−Oxtoby theory. The new theory predicts that a wavelength-dependent crossover in the temperature dependence is also possible in the barrierless isomerization reactions, in addition to the viscosity-mediated turnover. These crossovers are explained in terms of a shift in the rate governing the process from relaxation in the excited-state potential energy surface to the rate of the $S_1 \rightarrow S_0$ radiationless transition in the sink region. In the experimental investigations, the appearance of viscosity-mediated crossover in the temperature dependence of the decay rate and the absence of wavelength-mediated turnover is shown to reflect the steepness of the reactant ground-state potential surface. Analysis of rhodopsin isomerization suggests the short nuclear motion in the S_1 surface to be the major reason for the speed of isomerization observed. A low solvent relaxation time is predicted for the isomerization of rhodopsin, and the dynamics is expected to be viscosity-independent. A comparison between rhodopsin and isorhodopsin is also made, and an explanation for the slow dynamics in isorhodopsin is presented. Furthermore, our formalism helps in understanding the conflicting reaction mechanisms such as that in crystal violet. The results of the present study are expected to be relevant in understanding the dynamics of activationless isomerization reactions.

The organization of the rest of the paper is as follows. In the next section, we present the theoretical formulation of the barrierless reaction. The numerical results are presented in section III, along with a discussion of several specific experimental systems. Section IV concludes with a summary.

II. Generalized Theory of Barrierless Reactions

We start with the standard non-Markovian generalized Langevin equation, which describes the velocity (u) of a solute

in a one-dimensional harmonic potential well under the influence of a stochastic force, $f(t)$

$$\dot{u}(t) = -\omega^2\chi(t) - \int_0^t \zeta(t-\tau)u(\tau)\,d\tau + \frac{1}{m}f(t) \qquad (1)$$

where $\dot{u}(t)$ and $u(t)$ represent the accelaration and velocity, respectively. Equation 1 is associated with the fluctuation−dissipation relation

$$\langle f(t)f(\tau)\rangle = \langle f(t-\tau)f(0)\rangle = k_B T m\zeta(|t-\tau|) \qquad (2)$$

where ω is the frequency of the excited potential surface, $\zeta(t-\tau)$ is the memory kernel of friction, T is the temperature, and k_B is the Boltzmann constant.

For a harmonic surface, the generalized Langevin equation can be transformed into a generalized Smoluchowski equation with a time-dependent diffusion coefficient, $D(t)$, defined by[17]

$$D(t) = \frac{-k_B T}{m\omega^2}\frac{d\ln\xi(t)}{dt} \qquad (3)$$

where $\xi(t) = L^{-1}\hat{\xi}(z)$ is given as

$$\hat{\xi}(z) = \frac{1}{z + \omega^2\hat{\vartheta}(z)} \qquad (4)$$

and

$$\hat{\vartheta}(z) = \frac{1}{z + \hat{\zeta}(z)} \qquad (5)$$

$D(t)$ can be obtained from the time-dependent friction, $\xi(t)$. However, to find $\hat{\vartheta}(z)$ we need to know the frequency-dependent friction, $\hat{\zeta}(z)$. Note that one could also derive a generalized Fokker−Planck equation where the probability distribution function would depend both on the position and the velocity of the solute. The solution of such an equation would certainly contain more detailed dynamical information than the generalized Smoluchowski equation. However, solution of the generalized Fokker−Planck equation would involve extensive numerical work. The advantage of the generalized Smoluchowski equation with the time-dependent diffusion coefficient is that while it is exact for the harmonic surface, it also contains some (but not all) of the effects of underdamped motion in a simplified description. That is, no oscillations on the potential energy surface are considered near the minima. The oscillations arise only when friction is less (underdamped). To circumvent this difficulty, different relaxation times are employed where the fast time scale (low friction) relaxes faster until the minimum of the excited potential energy surface (S_1) and from there on a very slow relaxation (high friction) takes over. Thus, using this overdamped description itself, a realistic model is constructed. Such considerations are quite common in the study of barrierless electron-transfer literature,[21,24] and this assumption is transparent and does not sacrifice any interesting results. Now it is interesting to inquire whether the fast and slow relaxation times are realistic? The answer is yes; the friction that enters the generalized Langevin equation is bimodal in nature.[22] There is an ultrafast part that essentially arises from the dynamics of the solute in the cage formed by the surrounding solvent molecules. The second contribution to the translational friction originates from the coupling of the solute motion to the collective density fluctuations of the solvent. The coupling to the density fluctuation is responsible for the relaxation of the cage and has a long time decay.

Previous works on the generalized Smoluchowski equation used time-dependent $D(t)$ derived from the exponential memory kernel with a single relaxation time constant. However, the actual friction, $\zeta(t)$, is generally a bimodal function and shows variety with varying parameters. Having this in mind, we examine the dynamics of isomerization using a fairly realistic model for the molecular level, time-dependent friction experienced by the reacting system in its passage down the potential curvature. We have used two different expressions for the $\zeta(t)$. These two expressions are

$$\zeta(t) = \zeta(t=0)\frac{\cos(t/4\tau_1)}{\cosh(4t/\tau_2)} \qquad (6)$$

$$\zeta(t) = \zeta(t=0)\{A\exp(-t/\tau_1) + (1-A)\exp(-t/\tau_2)\} \qquad (7)$$

where τ_1 and τ_2 are the relaxation time constants for the ultrafast and slow components, respectively, and $\zeta(t=0)$ denotes the zero time friction. Equation 7 also shows another form for friction using a simple biexponential form, where A represents the weight factor. Equation 6 or 7 can be used as the friction expression to calculate the time-dependent diffusion coefficient and the isomerization rate constant. We shall refer to the calculations based on eqs 6 and 7 as model I and model II, respectively. Clearly they describe two different situations. Equation 6 is appropriate for simple liquids, while eq 7 might be appropriate in more complex situations. As already emphasized, the times τ_1 and τ_2 have different origins and can be vastly different. While model I seems to explain the friction behavior more close to the mode coupling theory results, most of the experimental results are analyzed using the biexponential relaxation times, and hence, studying the system with model II will be a convenient reference point. Note here that the above friction models are more suitable when the isomerizing group carries no or diffused charge. When an isomerizating group having a localized charge is considered in a polar solvent, the rotating charge will experience an enhanced drag due to the coupling of the charge with the polarization mode (ion−dipolar Coulombic interaction) of the solvent. This extra friction due to the strong dielectric forces is not considered in eqs 6 and 7 and, hence, is a limitation of our model. Several interesting theories have been developed by van der Zwan and Hynes[25] to study the isomerization of ionic solutes in polar solvents. In these studies, the role of solvent friction has been studied comprehensively.

The use of two desparate relaxation time constants in the friction expression has been justified by several experimental analysis. Ippen et al.[26] and Cremer and Windsor[27] while studying the ground-state recovery of malachite green have concluded more than one exponential is required to fit their excited-state absorption and ground-state recovery data. In addition, Hirsch and Mahr[28] have shown that the excited-state population decay curve of malachite green fits well only with the double-exponential form with two different decay times. Fluorescence decay of crystal violet was investigated by Beddard et al.,[29] and they also had a similar conclusion. Further, femtosecond experiments by Peteanu et al.[9] on the isomerization of rhodopsin confirm the nonsingle-exponential decay of different relaxation times.

More recently, Zhang et al.[30] studied the barrierless isomerization dynamics of cyanine dye, 3,3′-bis(3-sulfopropyl)thiacyanine triethylaminium salt, in various viscous alcohol solvents and explained the origins of two decay components in the relaxation dynamics. Their results show that the slower component time constant (τ_2) increases to several tens of

picoseconds when the solvent is varied. However, the faster time constant (τ_1) remains relatively unchanged.

The rate parameter relationship with viscosity is studied frequently in the experimental analysis of activationless electronic relaxations. In the theoretical analysis, however, friction is usually considered, and it is related to the rate constant. The obtained results were analyzed assuming a linear relationship between friction and viscosity. It is interesting here to note that friction originates from the solute−solvent two-body interaction and it is a microscopic quantity, whereas macroscopic viscosity is solely a solvent property. It is unfortunate and indeed frustrating that no such accurate relationship exists; thus, we restrict ourselves to the simple approximation suggested by Stokes−Einstein. As mentioned earlier, friction in our analysis originates from two different sources and their relation with the viscosity is important in understanding the rate constant dependence on the solvent parameter. Rigorously speaking, the binary collision term does depend on the solvent structure via $g(\sigma)$ and, hence, on viscosity. Since it does not couple to the solute−solvent two-particle direct correlation function, the viscosity dependence is very weak. On the contrary, long time dynamics is coupled to both the structure factor and also to the two-particle direct correlation function which governs the viscosity. Thus, the long time relaxation shows a overwhelming viscosity dependence compared to that of short time relaxation. This picture holds good for the low and moderate density regions,[31] and only under very high densities and temperatures (near critical point) does the mode coupling theory based calculations[32] show a high viscosity dependence for the binary friction. Since most of the barrierless isomerization reactions are carried out under these low and moderate density conditions, it is safe to assume that only the long time or zero-frequency friction is related to the viscosity via the Stokes−Einstein relation.

Note that the zero-frequency friction, $\zeta(z = 0)$, is obtained by the time integration over $\zeta(t)$. The important point here is that *while the value of $\zeta(z = 0)$ may be controlled by the slow time constant, τ_2, the rate of an ultrafast reaction can be coupled to the faster relaxation time, τ_1.* We need a non-Markovian theory to capture this aspect of the dynamics. Clearly, this itself can give rise to a fractional viscosity dependence of the reaction rate.

In the present work, the radiationless population decay is described via a coordinate-dependent sink, which is centered at the excited-state potential minimum. The Brownian motion of the initially excited molecule is governed by the force from the potential and also by the frictional forces offered by the solvent. This time-dependent diffusion in the higher harmonic surface can be conveniently described by the modified Smoluchowski equation description for the probability distribution $P(\chi,t)$, with a sink term as,

$$\frac{\partial P(\chi,t)}{\partial t} = \frac{\partial}{\partial \chi}\left\{D(t)\frac{\partial P(\chi,t)}{\partial \chi} + \frac{D(t)}{k_B T} m\omega^2 \chi P(\chi,t)\right\} - S(\chi)P(\chi,t) \quad (8)$$

Here $P(\chi,t)$ is the probability distribution at the χ coordinate and at time t, m denotes the effective mass, and ω represents the frequency of the harmonic well. The time-dependent diffusion coefficient coincides asymptotically with the long time diffusion coefficient (D) used in the conventional Markovian process; i.e., $D(t) = D$ as $t \rightarrow \infty$. $S(\chi)$ is the sink function, which is related to the local sink-transfer rate constant, k_s, at position χ_s by $S(\chi) = k_s\delta(\chi - \chi_s)$.

For any χ, the solution of the generalized Smoluchowski equation in the *absence* of sink is given by[21]

$$G(\chi,t/\chi_j,0) = \frac{(m\omega^2)^{1/2}}{[2\pi k_B T[1-\xi(t)^2]]^{1/2}} \exp\left[-\frac{m\omega^2[\chi - \chi_j\xi(t)]^2}{2k_B T[1-\xi(t)^2]}\right] \quad (9)$$

where χ_0 is the initial position of the solute at time $t = 0$. However, the solution of the generalized Smoluchowski equation in the presence of a delocalized sink is rather difficult to obtain. An efficient method that makes use of the above Green's function expression to solve eq 8 with delocalized sink has been discussed at length by Gayathri and Bagchi.[21] Both the time-dependent survival probability and the average rate need to be obtained numerically, although the latter is somewhat simpler. The final expression of the average rate is given by

$$k_I = \lim_{z\rightarrow 0} \frac{k_s \Delta G(\chi,\infty/\chi_0,0)}{1 + k_s[\Delta G(\chi,z/\chi_0,0) - \Delta G(\chi,z/\chi_s,0)]} \quad (10)$$

where $\Delta G(\chi,z/\chi_j,0)$ is in the form

$$\Delta G(\chi,z/\chi_j,0) = \int_0^\infty \exp(-zt)[G(\chi,t/\chi_j,0) - G(\chi,\infty/\chi_0,0)]\,dt \quad (11)$$

A special model that has been widely used in the study of barrierless reactions assumes that the reaction occurs with unit probability when the reactant arrives at a specific location, for example, the minimum of the potential energy surface. This may be modeled by placing a pinhole sink at the minimum of the excited-state surface.[15] Then eq 8 can be exactly solved by the method of images under appropriate initial boundary conditions.[15]

$$P(\chi,t) = \frac{(m\omega^2)^{1/2}}{[2\pi k_B T[1-\xi(t)^2]]^{1/2}}\left\{\exp\left[-\frac{m\omega^2[\chi + |\chi_0|\xi(t)]^2}{2k_B T[1-\xi(t)^2]}\right] - \exp\left[-\frac{m\omega^2[\chi - |\chi_0|\xi(t)]^2}{2k_B T[1-\xi(t)^2]}\right]\right\} \quad (12)$$

The survival probability at the excited surface can be written as

$$P_e(t) = \int_0^\infty P(-\chi,t)\,d\chi = \int_{-\infty}^0 P(\chi,t)\,d\chi \quad (13)$$

Equations 10 and 13 are employed in our calculation of the rate constant and survival probability for the barrierless isomerization process. The significance of these quantities in the context of barrierless isomerization reaction is considered in the next section.

III. Results and Discussion

(a) Numerical Analysis. In this section, we describe and discuss the results obtained by numerical solution of the equations described in the previous section. All the quantities involved are made dimensionless prior to the calculations. We have scaled time by picoseconds and the distance by angstroms. The following array of values are employed in our calculations for both model I and model II: $\tau_1 = 0.05$ ps, $\chi_s = 0$, $T = 298$ K, $m = 100$ g/mol, and, for model II, $A = 0.65$. τ_2 has been varied to explore the effects of slow dynamics.

The effect of $D(t)$ with varying potential curvature for model I is represented in Figure 2. Figure 2 shows that $D(t)$ varies linearly with t at short time as expected from eq 3. This increase

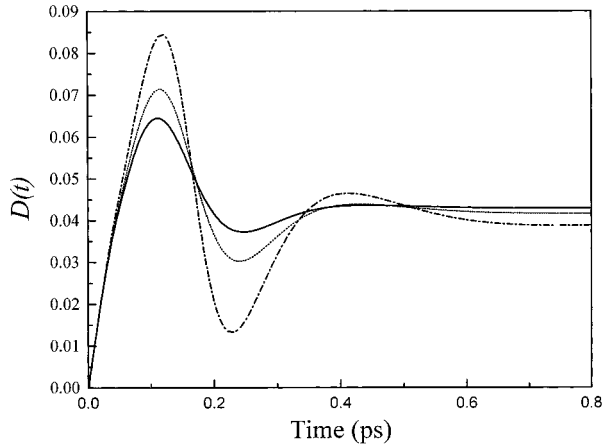

Figure 2. Calculated time-dependent diffusion coefficient ($D(t)$), plotted as a function of time (t) in picosecond at three different harmonic curvature potentials, $\omega^2 = 10$ (solid line), 50 (dotted line), and 100 (dash−dot line). Equation 6 is employed for the time-dependent friction (model I) to calculate the $D(t)$ values. The values of solvent relaxation time constant (τ_2) and zero time friction ($\zeta(t = 0)$) are 0.2 and 320, respectively. All the parameters involved are in dimensionless units. See text for details.

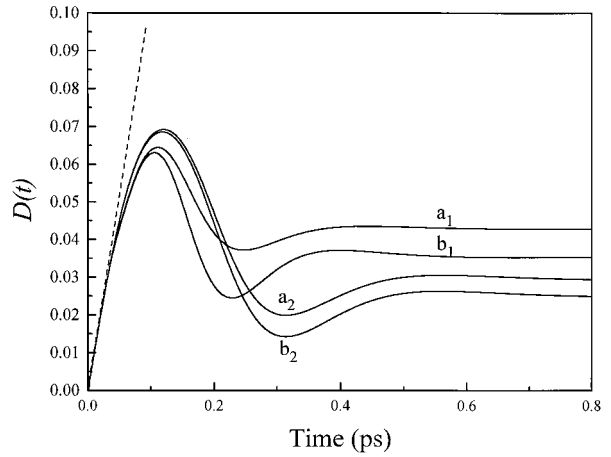

Figure 3. Plot of the time-dependent diffusion coefficient, $D(t)$, as a function of time, t, for four different cases: (a_1) model I, $\tau_2 = 0.2$; (b_1) model I, $\tau_2 = 0.25$; (a_2) model II, $\tau_2 = 0.2$; (b_2) model II, $\tau_2 = 0.25$. The dashed line represents the diffusion coefficient values calculated for the frictionless case using eq 15 as discussed in the text. In this figure, the effect of solvent time relaxation constants due to density fluctuation and binary collision on the diffusion coefficient has been compared. In addition, the effect of inertial behavior on the time-dependent diffusion coefficient can be studied. The value of ω^2 employed is 10. The values of the other fixed parameters are the same as those used to obtain the results in Figure 2.

in $D(t)$ is independent of the frequency employed. The change in the potential curvature, however, influences the asymptotic D_∞ value and the transient maxima observed. The fact that increasing ω decreases D_∞ suggests that as the potential barrier becomes steeper, coupling to the solvent is reduced. A detailed study of the effect of potential curvature on the time-dependent diffusion coefficient was carried out by Morita and Bagchi[33] for the bimolecular reactions.

A comparison between model I and model II is made in Figure 3 for two different values of τ_2. As can be seen, model I has more of a decrease in the transient maximum than model II. However, the asymptotic diffusion coefficient is considerably higher for model I than for model II. A similar $D(t)$ maxima and a lower D_∞ value predict the isomerization rate constant to be lower for model II. Figure 3 also shows that the decay from the short time maxima to the asymptotic value is reached much faster for model I. The D_∞ variation for different τ_2 values shows that a small change in τ_2 has a larger effect on the asymptotic $D(t)$ for model I than for II. This higher dependence of D_∞ on τ_2 is expected to have a greater influence of solvent viscosity for model I than for model II.

Further analysis of Figure 3 suggests that we can separate contributions to $D(t)$ arising from frictionless and different frictional sources. This is achieved by comparing the temporal behaviors of $D(t)$ for different values of τ_2 and studying the diffusion in the absence of friction. First, under frictionless conditions, i.e., when $\zeta(t) = 0$, eq 4 can be written as

$$\xi(z) = \frac{z}{z^2 + \omega^2} \tag{14}$$

Taking the inverse Laplace transform of (14) and substituting in eq 3, we obtain an expression for the time-dependent diffusion coefficient that depends only on the mass, potential curvature, and temperature.

$$D(t) = \frac{k_B T}{m\omega} \tan(\omega t) \tag{15}$$

Equation 15 describes the time-dependent $D(t)$ in the absence of friction, and it is generally considered to be due to the inertial motion of the particle.[34] The total time dependence and the frictionless diffusion coefficients are plotted for comparison in Figure 3. It is clearly shown that the initial raise in $D(t)$ is dominated by the inertial motion along the potential surface. Note here that such inertial motion is free from solvent viscosity.

In addition to inertial motion, diffusion is also influenced by the two different frictional forces, namely, binary collisions and density fluctuations. As mentioned earlier, the relative contributions to the binary and density fluctuation terms are controlled by the relaxation time constants, namely, τ_1 and τ_2, respectively. A further study of the temporal behavior of $D(t)$ is achieved by comparing $D(t)$ obtained for different τ_2 values. In Figure 3, a comparison of curves a_1 and b_1 for model I showed a marked difference in $D(t)$ at longer times for varying τ_2 values. A similar feature can be seen between curves a_2 and b_2 for model II as well. This suggests that the friction due to density coupling affects the diffusion dynamics only at the longer times. At short times, however, only a very little variation (this is more clearly visible for curves a_2 and b_2) is seen, thus indicating indirectly the role of binary friction. Hence, the time profile of $D(t)$ suggests the initial transient diffusion is governed by the inertial motion and binary friction, and the asymptotic D_∞ is, in turn, attributed to the density coupling to the solvent friction. An important point here is that diffusion due to binary friction is assumed to be independent of solvent viscosity under the low and moderated densities considered (as described in section II). Thus, a chemical reaction occurring at a fast time scale is expected to have viscosity independence.

The time-dependent survival probability on the excited surface is obtained for ω and $\zeta(t = 0)$ values of 1×10^{13} s^{-1} and 320, respectively, assuming a pinhole sink. Figure 4 illustrates a few representative calculations for different τ_2 values for model I. At low τ_2 values (≤ 0.2), the decay curves have two regions with different slopes. A noteable feature here is that at short time the decay is rather slow and at longer times the decay becomes rapid. At higher τ_2 values (≥ 0.3), the nonradiative decay is very slow although still retains the features. Figure 4 also shows these short time slow and long time fast decays to be a function of τ_2.

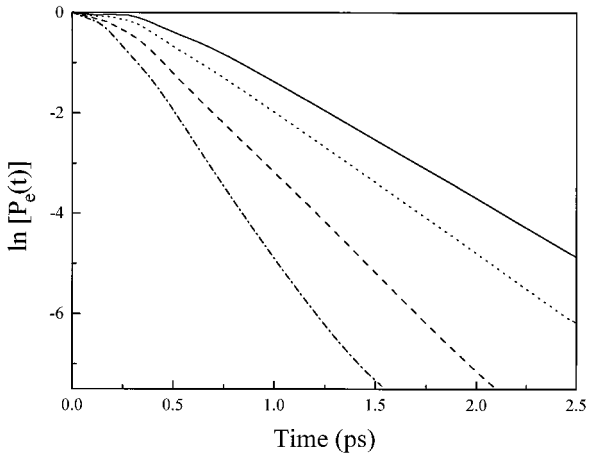

Figure 4. Effect of solvent relaxation time constant due to density fluctuations (τ_2) on the excited-state population. The logarithmic values of the survival probability, $P_e(t)$ obtained using model I are plotted as a function of time in picoseconds. The calculations for $P_e(t)$ are performed for the pinhole sink at different solvent relaxation time constant values, $\tau_2 = 0.15$ (dash−dot line), $\tau_2 = 0.2$ (dashed line), $\tau_2 = 0.3$ (dotted line), and $\tau_2 = 0.5$ (solid line). The potential curvature and zero time friction considered here are $\omega = 1 \times 10^{13}$ s^{-1} and $\zeta(t = 0) = 320$. For calculational details, see the text.

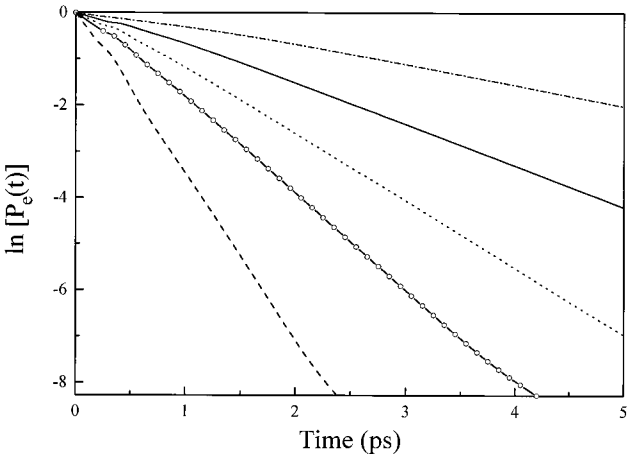

Figure 5. Time profile of the survival probability. The calculations are performed using the biexponential form for the time-dependent friction (model II). Various curves are for different values of the relaxation time constant values, $\tau_2 = 0.1$ (dashed line), $\tau_2 = 0.2$ (solid line with open circles), $\tau_2 = 0.3$, (dotted line), $\tau_2 = 0.5$ (solid line), and $\tau_2 = 1.0$ (dash−dot line). The weight factor value is chosen as 0.65, and the harmonic potential curvature and zero time friction values are the same as in Figure 4. See text for details.

Figure 5 represents the decay curve, $P_e(t)$, for model II for different τ_2 values. The features of this plot are very similar to those of Figure 4, but the decay is much slower than for model I. The rapid decay in model I can be attributed to the faster diffusion of the excited-state population predicted by model I. This effect can be seen from Figure 3, where the long time $D(t)$ is much higher than that for model II. Figures 4 and 5 also show a strong coupling of the survival probability to τ_2 as expected for a pinhole sink.[35]

A comparison of the survival probability variation between the Bagchi−Fleming−Oxtoby (BFO) model and the present non-Markovian analysis is shown in Figure 6. As the figure indicates, the population decay is much faster than in the Markovian case, suggesting the excited-state population has mostly decayed even before the steady state is reached. Thus, the effects of the short time motion are strongly felt for a pinhole sink. In fact, the above analysis removes a limitation of the

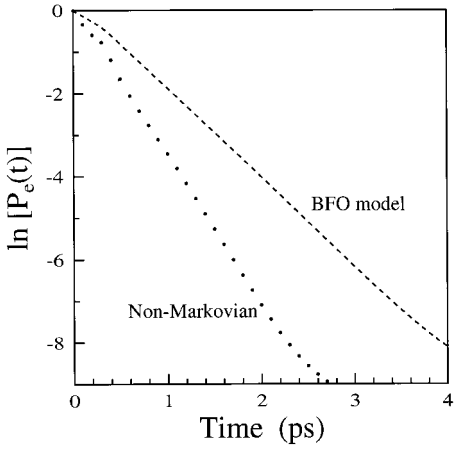

Figure 6. Decay of the excited-state population for the Bagchi−Fleming−Oxtoby (BFO) model (dotted line) and the present non-Markovian analysis (closed circles). The curves are obtained for the same zero-frequency friction, $\zeta(z = 0)$, value of 20; i.e., both systems are chosen to have the same long time diffusion coefficient. Equation 7 is employed for the time integration for zero-frequency friction in the non-Markovian case. Refer to the text for discussion.

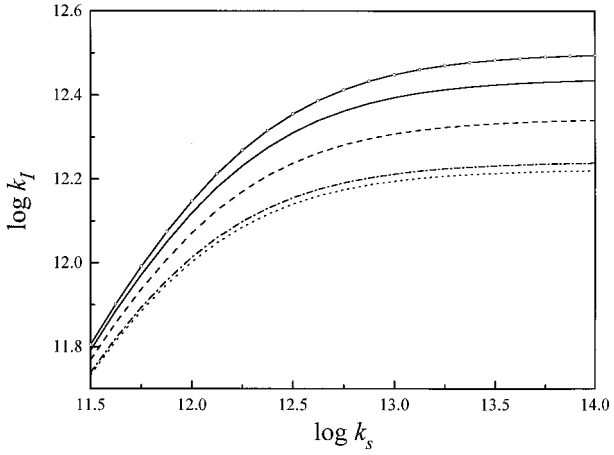

Figure 7. Calculated values of the average rate constant, k_I, using model I plotted as a function of $S_1 \rightarrow S_0$ sink-transfer rate constant, k_s in the logarithmic scale. Various curves are obtained for different τ_2 values of 0.1 (solid line with open circle), 0.2 (solid line), 0.3 (dashed line), 0.5 (dash−dot line), and 1.0 (dotted line). The values of the potential curvature, ω, initial excitation position, χ_0 and zero time friction, $\zeta(t = 0)$, are respectively 1×10^{13} s^{-1}, 0.5, and 320. All the quantities involved are dimensionalized prior to the calculations as discussed in the text. Refer to the text for details regarding calculations.

previous pinhole sink model which could never explain the decoupling of the reaction rate from the solvent shear viscosity.[15] Assuming the Stokes−Einstein equation to be valid, the constant $\zeta(z = 0)$ condition essentially ensures that the viscosity of the system remains the same. These curves illustrate a much slower decay in the excited-state population for the previous BFO analysis where the time-independent diffusion is assumed compared to the non-Markovian result. Though the asymptotic diffusion coefficient remains the same for both cases, the reason for the faster decay in the non-Markovian case is related to the transient diffusion which arises from the short time ultrafast relaxation component (cf. Figure 2).

The combined effects of k_s and τ_2 on the dynamics of barrierless isomerization are shown in Figure 7. The reported curves are obtained using model II, and the features of the curves remain the same when model I is employed as well. However, for model I, slightly higher values of k_I are observed for similar τ_2 and k_s values. Figure 7 shows, for a fast sink transfer (high

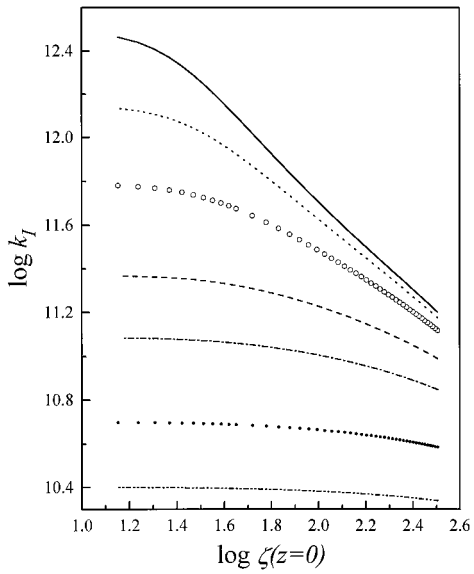

Figure 8. log−log plot of the isomerization rate constant, k_I, versus the zero-frequency friction for different values of the sink-transfer rate, k_s. The k_I values employed in the calculation are 100 ps^{-1} (solid line), 1 ps^{-1} (dotted line), 0.3 ps^{-1} (open circles), 0.1 ps^{-1} (dashed line), 0.05 ps^{-1} (dash−dot line), 0.01 ps^{-1} (dash−dot−dot line). The zero-frequency friction is calculated by time integration over the biexponential form of the time-dependent friction, $\zeta(t)$ (model II). The plot shows a decrease in the k_s value correspondingly decreases the rate constant dependence on zero-frequency friction. As mentioned in the text, the zero-frequency friction is related directly to the solvent viscosity. The generalized relationship between the barrierless isomerization rate constant and zero-frequency friction can be written as $k_I = A(\zeta(z=0))^{-\alpha}$. For high sink-transfer rate of 100 ps^{-1}, $\zeta(z=0)$ is shown to vary inversely with a α of 1. And for low k_s values, curves show a much reduced α value, indicating fractional dependence. Thus, a weak viscosity dependence of the reaction rate is expected. Note here that for very low sink-transfer rate, the isomerization dynamics is completely independent of zero-frequency friction and, hence, k_I is decoupled from solvent viscosity.

k_s), the plots diverge for different values of τ_2. As noted earlier, the zero-frequency friction is coupled mainly to the slower of the two time constants of the time-dependent friction, that is, the one arising from the collective density fluctuation (τ_2). This implies that at higher k_s values, the average rate constant (k_I) is strongly dependent on the zero-frequency friction and, hence, on the solvent viscosity. At low k_s, all the curves almost converge, indicating weak viscosity dependence of k_I. Figure 7 thus predicts the nontrivial role played by the sink-transfer rate on the barrierless isomerization reaction dynamics.

The role of the time constant due to solvent density fluctuation on the dynamics of barrierless isomerization reactions can also be envisaged from Figure 7. For a fixed value of the sink-transfer rate constant, k_I decreases with increasing τ_2 value. A comparison of the effects of low and high values of τ_2 on k_I shows a larger dependence of k_I for the former case, thus suggesting the dependence of the isomerization rate constant on the density fluctuational time constant progressively decreases as the τ_2 value is increased. This indicates that the effect of viscosity on the isomerization dynamics is less pronounced when the time constants between the ultrafast and slow components differ largely. Thus, for slow viscous liquids with vastly different τ_1 and τ_2 values, viscosity decoupling is expected. And as discussed earlier, this feature is influenced greatly by k_s.

It is interesting to envisage the role of $\zeta(z=0)$ on the rate of isomerization process. Figure 8 shows the variation of k_I with $\zeta(z=0)$ for different values of k_s. An increase in zero-frequency friction essentially hinders the diffusive motion of the excited

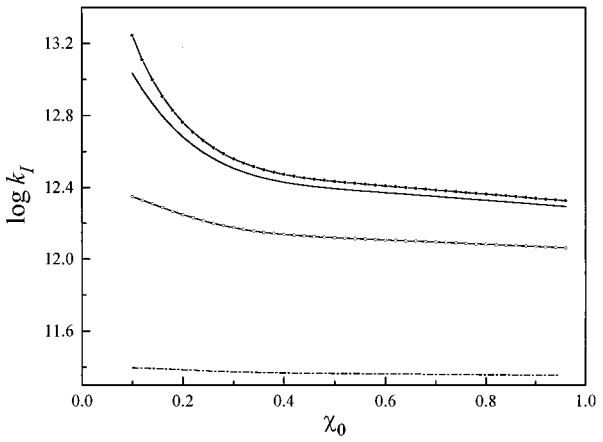

Figure 9. Semilog plot showing the dependence of the average rate constant (k_I) with the initial excitation position (χ_0) for different sink-transfer rate constant values, $k_s = 1 \times 10^{14}$ s^{-1} (solid line with closed circle), $k_s = 1 \times 10^{13}$ s^{-1} (solid line), $k_s = 1 \times 10^{12}$ s^{-1} (solid line with open circle), and $k_s = 1 \times 10^{14}$ s^{-1} (dash−dot line). The calculations are made for the solvent density fluctuational time constant, τ_2, value of 0.2 using model I for the time-dependent friction. The values of the other fixed parameters are the same as those used to obtain the results in Figure 6. Refer to the text for details regarding the calculations.

wave packet, and the isomerization rate constant is expected to decrease. This is observed at higher sink-transfer rate constant values. Note also that the isomerization rate constant is independent of k_s under this condition. The reason for this is the diffusion in the harmonic surface is the rate-limiting process at this high sink-transfer rate condition, friction has a large effect, and the change in k_s has no influence. At the low sink-transfer rate ($k_s \leq 1 \times 10^{11}$ s^{-1}), the change in friction does not really show any significant change in k_I. However, the k_I value decreases with decreasing k_s, suggesting the overall isomerization dynamics is controlled by the sink transfer.

The dependence of the population relaxation on the wavelength of the excitation light enters in our model through the initial distribution position (χ_0) on the excited-state potential surface (S_1). When the sink transfer is rapid, the nuclear relaxation in the S_1 surface governs the overall rate, and hence, the initial excitation position greatly influences k_I. Figure 9 indicates k_I is inversely related to χ_0, suggesting longer wavelength excitation pulses will have a higher isomerization rate. However, when the population transfer at the sink position is slow ($k_s \leq 1 \times 10^{11}$ s^{-1}), the relaxation process becomes completely independent of the excitation wavelength. Both the wavelength dependence and the independence have been observed experimentally.[36−40]

Figure 10a reproduces the central tenets of the BFO[15] model with regard to the relationship between the isomerization rate and the reciprocal of temperature. The Arrhenius plot calculations for the k_s value of 1×10^{12} s^{-1} depicted in Figure 10a clearly show a crossover from positive to negative activation energy for decreasing values of τ_2. The physical process underlying the solvent-mediated crossover can be explained based on the shift in the rate-governing process involved. When the population of the excited state is prepared, the overall process that takes the distribution to the ground state involves the motion of the wave packet at the excited potential energy surface and relaxation at the sink point as well. The diffusive motion of the wave packet in the excited state depends on the frictional forces that act as resistance and also on the potential curvature. This resistive frictional force acts against the bond-twisting process which is essential for the formation of the other isomer. Physically, as the temperature increases, the kinetic energy of

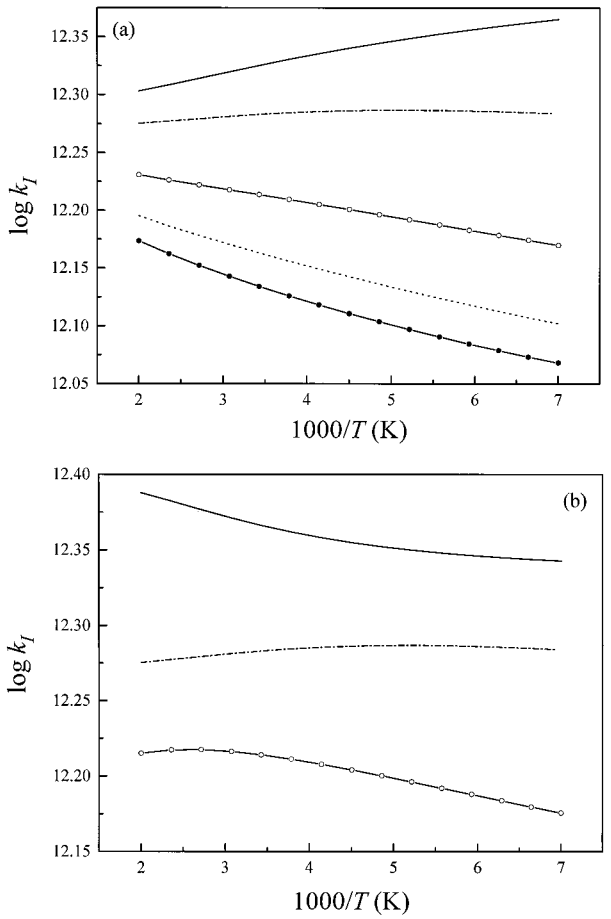

Figure 10. Temperature dependence of the nonradiative decay rate showing the crossover from negative to positive activation energy as the value of the solvent relaxation time constant, τ_2, and initial excitation position, χ_0, are varied. The calculated values are for model I. The values of potential curvature zero time friction are the same as those in Figure 5. (a) Arrhenius plot for $k_s = 1 \times 10^{12}$ s^{-1} and $\chi_0 = 0.5$. The curves are calculated for τ_2 values of 0.1 (solid line), 0.2 (dash−dot line), 0.3 (solid line with open circle), 0.4 (dotted line), and 0.5 (solid line with closed circle). (b) Arrhenius plot obtained for τ_2 and k_s values of 0.2 ps and 2.5×10^{12} s^{-1}, respectively. The various curves obtained are for the initial excitation position, χ_0 values of 0.3 (solid line), 0.5 (dash−dot line), and 0.9 (solid line with open circle). See the text for details.

the molecule also increases, which accelerates the rotation between the carbon−carbon bond. In other words, the increase in temperature helps the excited population to reach the minimum of the excited state more rapidly. Thus, when the diffusive motion of the molecule in the excited S_1 surface becomes rate limiting, the bond-twisting process has a positive temperature dependence.

At low τ_2, the diffusive nuclear motion is rapid compared to the sink transfer and the transfer from the excited S_1 surface to the ground S_0 state becomes the rate-governing process. An increase in temperature under this condition accelerates further the nuclear motion, and the population gets accumulated at the excited-state minimum. In addition, the population distribution around the sink point becomes broad at higher temperatures. Thus, an increase in broad distribution above the sink decreases k_I and leads to a negative temperature dependence.

A similar crossover in temperature dependence is also observed when the wavelength of the excitation light is increased (cf. Figure 10b). Such wavelength-mediated turnover from negative to positive activation energy in the Arrhenius plot is not been reported theoretically. The origin for this crossover in the temperature dependence is also attributed to the shift in the rate-governing process from the diffusion of the wave packet in the harmonic surface to the $S_1 \rightarrow S_0$ radiationless relaxation. The significance of the present theoretical analysis to the recently obtained experimental results is briefly reviewed in the next section.

(b) Experimental Observations and Interpretations.

(i) Photoisomerization and Ground-State Potential Energy Surface. In the experimental investigations on TPM dyes[38−40] (crystal violet and ethyl violet) and 1,1′-diphenyl-4,4′-cyanine (1144C),[37] temperature-dependent crossover is observed in the Arrhenius plot when the viscosity is varied. As illustrated in the previous section (cf. Figure 10a), such turnover arises due to the change in the rate-determining step from relaxation in the excited surface (S_1) to the sink transfer. Near this viscosity value, wavelength-mediated crossover is also expected from Figure 10b. To our knowledge, no experimental results exist for such a turnover for varying excitation wavelengths. More recent data by Alvarez et al.[37] on 1144C photoisomerization at 7 cP for 450, 660, and 770 nm excitation show a similar trend. However, it requires further experimental confirmation.

The observation of viscosity-mediated temperature crossover and the absence of wavelength-mediated crossover in most of the experimental studies on the barrierless isomerization reaction suggest (i) a narrow S_0 surface potential curvature and/or (ii) internuclear separation between the reactant and the product ground-state minima to be far away. For the latter to be true, the wave packet is expected to move a relatively long distance on the excited-state potential energy surface before it encounters the sink to decay. Thus, the motion of the wave packet on the S_1 surface becomes rate controlling. Under this condition, the isomerization kinetics is expected to be strongly coupled to the solvent viscosity and the turnover in temperature dependence is not expected. In contrast, the experimental studies on TPM dyes[38−40] show a viscosity-mediated crossover in temperature dependence.

For the former case, however, when the ground-state potential energy surface is narrow, the change in excitation wavelength does not appreciable change χ_0 in the S_1 surface. Thus, even when a viscosity-dependent temperature crossover is observed, the Arrhenius plot does not show a change in temperature dependence for varying wavelengths. Reports on TPM dyes[39,40] seem to indicate this feature, and our theory predicts a narrow ground-state potential energy surface for these molecules. On the contrary, for a reactant molecule with a broad potential curvature, different excitation pulses can create the initial distribution at different positions in the excited S_1 surface. This indicates that the distance traveled by the wave packet can be controlled by the wavelength of the excitation pulse. Thus, by properly tuning the wavelength for a fixed viscosity, the crossover in temperature dependence is expected in the Arrhenius plot. As discussed earlier, such an observation is visible under close examination of Alvarez et al.[37] results for the 1144C molecule. Its ground-state surface is expected to be relatively broad. Our analysis thus suggests the wavelength-dependent turnover in activation energy provides valuable information concerning the structure of the ground-state reactant potential energy surface.

(ii) Decay Dynamics of Rhodopsin and Isorhodopsin. The time-resolved spectral dynamics of 11-cis to all-trans isomerization of rhodopsin is shown by Schoenlein and co-workers[9,41] to be complete within 200 fs. Experimental observations show that no red-shifted stimulated emission is observed in the time-resolved measurements, which suggests a rapid torsional motion

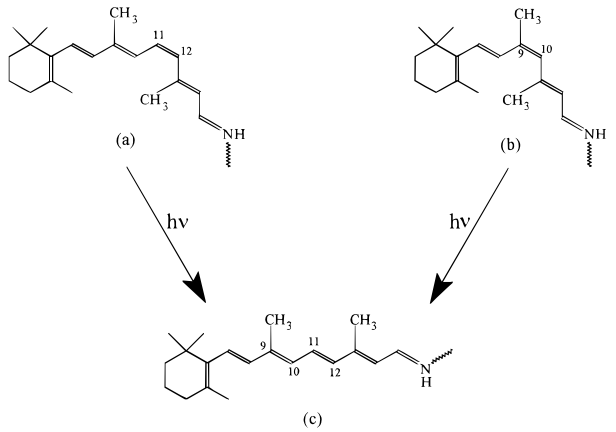

Figure 11. Schematic representation of the light-induced isomerization reactions of 11-*cis*-rhodopsin (a) and 9-*cis*-rhodopsin (isorhodopsin) (b) leading to the same photoproduct *all-trans*-bathorhodopsin.

of the excited species during its motion along the Franck−Condon region (low τ_1 and τ_2 values). Excited-state relaxation is shown to be of the order of 100 fs. This fast relaxation in the S_1 surface is further confirmed by resonance Raman intensity analysis as well.[42] Our model calculations show a fast sink transfer ($k_s = 1 \times 10^{14}$ s^{-1}) and short Brownian motion ($\chi_0 = 0.25-0.32$) along the excited-state surface to account for the observed 145−205 fs delay dynamics ($k_I \approx (6.8-4.9) \times 10^{12}$ s^{-1}) of rhodopsin.[43] These values have several implications. The low value of χ_0 suggests the isomerization should be independent of the viscous drag of the solvent particles. The short nuclear motion is justified by the resonance Raman studies,[44,45] indicating that the overall structural change associated with the isomerization is relatively small. A physical reason for this is the 11-*cis*-rhodopsin already exists in its twisted form along the reaction coordinate because of the steric interaction between the C-13 methyl and C-10 hydrogen groups.[46] In an earlier analysis by Wang et al.[47] on rhodopsin isomerization, excited-state vibrational coherence was invoked to account for the very low delay time observed. Our analysis here clearly shows that short-distance nuclear motion is also an important factor for this ultrafast femtosecond isomerization.

An interesting comparison can be made between the isomerization dynamics of rhodopsin and isorhodopsin (9-*cis*-rhodopsin). In contrast to rhodopsin, the isomerization in isorhodopsin occurs about the C_9-C_{10} double bond (cf. Figure 11). Nevertheless, the photoproduct of the 9-cis isomer is the same for *all-trans*-bathorhodopsin as that of rhodopsin. A schematic sketch of 9-*cis*-rhodopsin and the 11-*cis*-rhodopsin and the *all-trans* photoproduct (bathorhodopsin) is shown in Figure 11. Spectral measurements on isorhodopsin show a delay time of ∼600 fs, which is nearly 3 times longer than that for rhodopsin. Our theoretical calculations for the isorhodopsin isomerization for $\chi_0 = 0.5$ and $\tau_2 = 200$ fs suggest a time delay of 575−660 fs ($k_I \approx (1.7-1.5) \times 10^{12}$ s^{-1}) depending on the sink-transfer rate constant ($k_s = (2-1.5) \times 10^{12}$ s^{-1}).[48]

These calculations predict comparatively long distant nuclear motion, i.e., $\chi_0 = 0.5$ for isorhodopsin as opposed to 0.25−0.3 for rhodopsin. The high χ_0 value can also be attributed to the lack of any strong intramolecular nonbonded interactions that distort the polyene skeleton in the vicinity of the cis bond.[49] Our prediction of the relatively long distant motion in the S_1 surface for isorhodopsin is in good agreement with the photochemical quantum yield analysis[50] where the 9-cis isomerization shows a wavelength and temperature dependence while rhodopsin isomerization does not. This indicates the excited-state relaxation is the rate-limiting process in the isomerization dynamics of isorhodopsin. The wavelength dependence of the reaction also seems to indicate this fact.

In addition to the high χ_0 value (compared to the rhodopsin isomerization), the slow relaxation dynamics of isorhodopsin is attributed to the long time, slow component decay time constant, τ_2 from our theory. The high τ_2 value indicates that the excited-state electronic relaxation of isorhodopsin (9-cis isomer) is controlled by the slow excited-state dynamics. Recent experimental results[49] show that the excited-state absorption persists even after 150 fs for the 9-cis isomer. Note here that the S_1 surface absorption for rhodopsin is complete before 100 fs.[47] In addition, the spectral breathing of the stimulated emission of isorhodopsin[49] also indicates the wave packet motion in the S_1 surface is slower than in the rhodopsin case. Thus, the relatively long-lived excited-state absorption explains the high τ_2 value. A detailed viscosity variation study can give some useful insights. However, to our knowledge, such a study has not yet been carried out.

(iii) Conflicting Crystal Violet Isomerization Mechanism. Another interesting problem where the present theoretical analysis helps us in understanding the experimental results is in the isomerization dynamics of crystal violet. Lewis et al.[51] performed the absorption studies on crystal violet and suggested two ground-state conformers to be present under thermal equilibrium. They confirmed one isomer to have D_3 symmetry structure with all three phenyl rings tilted in one direction and proposed the other to have C_2 symmetry (one phenyl ring is tilted in the opposite direction). A schematic representation of these conformers is shown in parts a and b of Figure 12 . The proposed C_2 symmetry structure has been under constant study and debate for the past 5 decades now. In fact, the existence of two ground-state conformers itself has been questioned (cf. ref 11). Recently, Maruyama et al.[11] confirmed the presence of two ground-state isomers using femtosecond pump−probe measurements and predicted the other conformer to have a C_3 symmetry structure using molecular orbital calculations (cf. Figure 12c). Since experiments could not resolve this issue directly, indirect methods have been employed by both Lewis et al. and Maruyama et al. (in an attempt) to prove their proposed conformer.

Earlier Ben-Amotz and Harris[39] employed picosecond absorption spectroscopy and analyzed the delay time dynamics of crystal violet in linear alcohol series. The viscosity-mediated temperature crossover reported by these authors in higher alcohols can be confirmed from Figure 10a as arising due to the competition between S_1-state relaxation and sink transfer for rate governing.

Temperature-variation studies of Maruyama et al. on crystal violet isomerization in lower alcohol solvents indicate that the overall rate constant is independent of temperature. Even though only a small temperature range between 283 and 313 K has been studied, their results suggest from Figure 10b that the sink-transfer rate is comparable to or slightly less than the excited-state relaxation time constant in the lower alcohol solvents.

Wavelength dependence on the barrierless isomerization kinetics of crystal violet has also shown some interesting insights. Studies by Ben-Amotz and Harris[39] in ethanol, butanol, and octanol and by Sundström and Gillbro[40] in hexanol solvents show no indication of a wavelength dependence on the isomerization kinetics. This can be interpreted from Figure 9 as being due to the fast relaxation on the excited-state surface, thus suggesting the sink-transfer rate to be the rate-governing

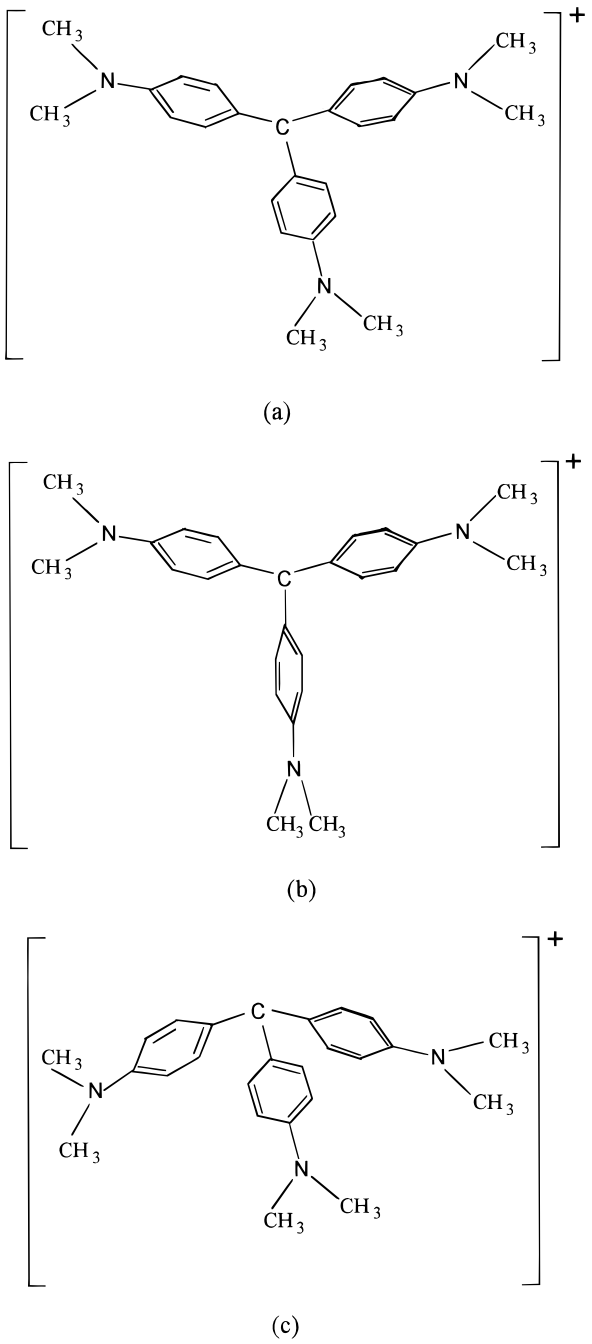

Figure 12. Proposed conformations of crystal violet in solution, (a) equilibrium ground-state conformer with D_3 symmetry (propeller structure) with all the phenyl rings tilted about the same molecular plan, (b) distorted propeller structure with C_2 symmetry suggested by Lewis et al.[51] as the other ground-state isomer, and (c) symmetry-breaking C_3 pyramidal structure proposed by Maruyama et al.[1] as a solvation isomer to the propeller D_3 structure (a).

step in the crystal violet isomerization, as discussed previously in this section.

An important observation that invoked C_3 symmetry structure as the unidentified conformer is the viscosity independent of the relaxation rate observed by Maruyama et al.[11] It is clear from the above discussion that k_s is less than the wave packet relaxation rate in the excited-state surface. In our theoretical model, Figures 7 and 8 clearly predict such viscosity independence does not necessarily mean there is no torsional motion of the phenyl group in the excited S_1 surface but instead only indicates a slow $S_1 \rightarrow S_0$ transfer rate constant. Thus, our study resolves all the experimental findings that appeared controversial in the crystal violet isomerization and suggests the C_3 symmetry structure (Figure 12a) proposed by Maruyama et al. due to viscosity independence alone to have some caveats.

IV. Conclusions

In this article, we have presented a generalized theory for the barrierless isomerization reaction in viscous liquids. The theory is based on a non-Markovian dynamics of the solvent frictional response. The time dependence of the diffusion coefficient for motion along the reaction coordinate has been incorporated via a time-dependent friction. The friction was modeled using two different models having two different relaxation time constants to account for the ultrafast and slow relaxations. The calculated $D(t)$ vs t curves for both of the models have features similar to the mode coupling theory results obtained recently. It is shown that in some cases the kinetics of excited-state twisting could be dominated by only the short time dynamics of the solvent. This is clearly because these reactions are themselves very fast, and they probe only the short time dynamics of the solvent which is often dominated by the binary, collisional events in the liquid.

The relevance of the present study can be appreciated if we recall that in all the existing studies of the barrierless reactions, a Markovian description of the diffusion coefficient was employed. In such a description, only the asymptotic, long time value of $D(t)$ (and hence of friction) controls the reaction. This naturally leads to a strong coupling between the isomerization reaction and the viscosity. However, in many cases, the reaction can be complete before the long time response of the solvent is felt by the reaction.

The diffusion that drives the reaction may have nothing to do with the measured viscosity of the medium. It has been discussed here that the ultrafast part of solvent response could have manifested itself in several important isomerization reactions. In addition, the present theoretical formalism predicts that the wavelength-dependent temperature crossover is possible and the reason for such turnover is traced back to the change in the rate-governing process from diffusion in the excited surface to the rate of sink transfer. The importance of the present study to understand the *mechanism of ultrafast isomerization reactions* has been pointed out. The contradictory mechanism of crystal violet isomerization has been taken as an example, and the applicability of the present theory has been demonstrated. The present theory also seems to help us understand the time course of rhodopsin and isorhodopsin isomerization which has been the subject of extensive research in recent years. The present theory suggests that a small nuclear motion of the excited rhodopsin could be the reason for the very low delay time observed experimentally.

Acknowledgment. It is a pleasure to thank Dr. Ranjit Biswas, Dr. N. Gayathri, and Ms. Sarika Bhattacharyya for their help and discussions. We also thank Mr. Rajesh K. Murarka and Mr. G. Srinivas for help with the manuscript. This work was supported in parts by grants from the Department of Science and Technology (DST, India) and by the Theoretical Chemistry Institute at the Department of Chemistry, University of Wisconsin, Madison.

References and Notes

(1) Vos, M. H.; Rappaport, F.; Lambry, J.-C.; Breton, J.; Martin, J.-L. *Nature (London)* **1993**, *363*, 320.
(2) Barbara, P. F.; Walker, G. C.; Smith, T. P. *Science* **1992**, *256*, 975.
(3) Kramers, H. A. *Physica* **1940**, *7*, 284.

(4) Grote, R. F.; Hynes, J. T. *J. Chem. Phys.* **1980**, *73*, 2715.
(5) Pollak, E. *J. Chem. Phys.* **1986**, *85*, 865.
(6) Wald, G. *Science* **1968**, *162*, 230.
(7) Yoshizawa, T.; Wald, G. *Nature (London)* **1963**, *197*, 1279.
(8) Bagchi, B.; Fleming, G. R. *J. Phys. Chem.* **1990**, *94*, 9 and references therein.
(9) Peteanu, L. A.; Schoenlein, R. W.; Wang, Q.; Mathies, R. A.; Shank, C. V. *Proc. Natl. Acad. Sci. U.S.A.* **1993**, *90*, 11762.
(10) Hayward, G.; Carlsen, W.; Siegman, A.; Stryer, L. *Science* **1981**, *211*, 942.
(11) Maruyama, Y.; Ishikawa, M.; Satozono, H. *J. Am. Chem. Soc.* **1996**, *118*, 6257.
(12) Sension, R. J.; Repinec, S. T.; Szarka, A. Z.; Hochstrasser, R. M. *J. Chem. Phys.* **1993**, *98*, 6291.
(13) Lenderink, E.; Duppen, K.; Wiersma, D. A. *J. Phys. Chem.* **1995**, *99*, 8972.
(14) Todd, D. C.; Fleming G. R. *J. Chem. Phys.* **1993**, *98*, 269.
(15) Bagchi, B.; Fleming, G. R.; Oxtoby, D. W. *J. Chem. Phys.* **1983**, *78*, 7375.
(16) Bagchi, B.; Oxtoby, D. W *J. Chem. Phys.* **1983**, *78*, 2735.
(17) Okuyama, S.; Oxtoby, D. W. *J. Chem. Phys.* **1986**, *84*, 5824.
(18) Schulten, K.; Schulten, Z.; Szabo, A. *Phys. A* **1980**, *100*, 599. (b) Szabo, A.; Lamm, G.; Weiss, G. H. *J. Stat. Phys.* **1984**, *34*, 225.
(19) Sebastian, K. L. *Phys. Rev. A* **1992**, *46*, R1732.
(20) Samanta, A.; Ghosh, S. K. *Phys. Rev. E* **1993**, *47*, 4568.
(21) (a) Gayathri, N.; Bagchi, B. *J. Phys. Chem.* **1996**, *100*, 3056. (b) Bagchi, B.; Gayathri, N. *Adv. Chem. Phys.* **1999**, *107*, 1.
(22) (a) Bhattacharyya, S.; Bagchi, B. *J. Chem. Phys.* **1997**, *106*, 1757. (b) *J. Chem. Phys.* **1997**, *106*, 7262.
(23) Hynes, J. T. *J. Phys. Chem.* **1986**, *90*, 3701.
(24) Bicout, D. J.; Szabo, A. *J. Chem. Phys.* **1998**, *109*, 2325.
(25) (a) van der Zwan, G.; Hynes, J. T. *J. Chem. Phys.* **1982**, *76*, 2993. (b) van der Zwan, G.; Hynes, J. T. *J. Chem. Phys.* **1983**, *78*, 4174. (c) van der Zwan, G.; Hynes, J. T. *Chem. Phys. Lett.* **1983**, *101*, 367.
(26) Ippen, E. P.; Shank, C. V.; Bergman, A. *Chem. Phys. Lett.* **1976**, *38*, 611.
(27) Cremers, D. A.; Windsor, M. W. *Chem. Phys. Lett.* **1980**, *71*, 27.
(28) Hirsch, M. D.; Mahr, H. *Chem. Phys. Lett.* **1979**, *60*, 299.
(29) Beddard, G. S.; Doust, T.; Windsor, M. W. In *Picosecond Phenomena II*; Hochstrasser, R. M., Kaiser, W., Shank, C. V., Eds.; Springer: New York, 1980; p 167.
(30) Zhang, T.; Chen, C.; Gong, Q.; Yan, W.; Wang, S.; Yang, H.; Jian, H.; Xu, G. *Chem. Phys. Lett.* **1998**, *298*, 236.
(31) (a) Biswas, R.; Bagchi, B. *J. Chem. Phys.* **1996**, *105*, 7543. (b) Dr. Ranjit Biswas, personal communication.
(32) Murarka, R. K.; Bhattacharyya, S.; Biswas, R.; Bagchi, B. *J. Chem. Phys.* **1999**, *110*, 7365.
(33) Morita, A.; Bagchi, B. *J. Chem. Phys.* **1999**, *110*, 8643.
(34) (a) We need to mention here that in Adelman's treatment[34b] of the diffusion problem such inertial effects is ignored and only frequency-dependent friction is assumed to control the diffusion dynamics. Hence, only the non-Markovian process is considered. Dong and Andre[34c] have shown later the importance of inertial motion in their work on diffusion-limited reactions, for the free particle. Recently, Morita and Bagchi[30] have studied the effects of inertial and the non-Markovian effects for both free particle as well as for the diffusion in the presence of a potential curvature. Several others have also studied the influence of inertial and non-Markovian dynamics on the collision-induced reactions.[34d] Note here this inertial effect is inborne in the derivation of Okuyama and Oxtoby.[17] (b) Adelman, S. A. *J. Chem. Phys.* **1976**, *64*, 124. (c) Dong, W.; Andre, J. C. *J. Chem. Phys.* **1994**, *101*, 299. (d) See, for example: Ibuki, K.; Ueno, M. *Bull. Chem. Soc. Jpn.* **1997**, *70*, 543.
(35) Roy, S.; Bagchi, B. *J. Chem. Phys.* **1994**, *100*, 8802.
(36) Åkesson, E.; Bergstrom, H.; Sundström, V.; Gillbro, T. *Chem. Phys. Lett.* **1986**, *125*, 385.
(37) Alvarez, J.-L.; Yartsev, A.; Åberg, U.; Åkesson, E.; Sundström, V. *J. Phys. Chem. B* **1998**, *102*, 7651.
(38) Ben-Amotz, D.; Jeanloz, R.; Harris, C. B. *J. Chem. Phys.* **1987**, *86*, 6119.
(39) Ben-Amotz, D.; Harris, C. B. *J. Chem. Phys.* **1987**, *86*, 4856.
(40) Sundström, V.; Gillbro, T. *J. Chem. Phys.* **1984**, *81*, 3463.
(41) Schoenlein, R. W.; Peteanu, L. A.; Mathies, R. A.; Shank, C. V. *Science* **1991**, *254*, 412.
(42) Loppnow, G. R.; Mathies, R. A. *Biophys. J.* **1988**, *54*, 35.
(43) The calculated values are from using model I. The values obtained from model II also seems to have a close agreement with these values. For model II, for χ_0 values of 0.25−0.32, the delay time is expected to be in the range of 150−210 fs ($k_l = (6.7-4.8) \times 10^{12}$ s^{-1}).
(44) Paulings, I.; Parcloen, J. A.; van der Berg, E.; Winkel, C.; Lugtenburg, J.; Mathies, R. A. *Biochemistry* **1987**, *26*, 2544.
(45) Warshel, A. *Nature (London)* **1976**, *260*, 679.
(46) Warshel, A.; Barboy, N. *J. Am. Chem. Soc.* **1982**, *104*, 1469.
(47) Wang, Q.; Schoenlein, R. W.; Peteanu, L. A.; Mathies, R. A.; Shank, C. V. *Science* **1994**, *266*, 422.
(48) Model I is used to calculated the delay time dynamics of isorhodopsin. The delay time values obtained using model II for the sink-transfer rate constant $k_s = (2.0-2.7) \times 10^{12}$ s^{-1} are 590−650 fs ($k_l = (1.7-1.5) \times 10^{12}$ s^{-1}).
(49) Schoenlein, R. W.; Peteanu, L. A.; Wang, Q.; Mathies, R. A.; Shank, C. V. *J. Phys. Chem.* **1993**, *97*, 12087.
(50) Hurley, J. B.; Ebrey, T. G.; Honig, B.; Ottolenghi, M. *Nature (London)* **1977**, *270*, 540.
(51) Lewis, G. N.; Mayel, T. T.; Lipkin, D. *J. Am. Chem. Soc.*, **1942**, *64*, 1774.